Eur. Phys. J. C 37, 185–195 (2004)
Digital Object Identifier (DOI) 10.1140/epjc/s2004-01980-4

THE EUROPEAN PHYSICAL JOURNAL C

On the possibility of measuring the gluon distribution in proton with "γ + jet" events at LHC

D.V. Bandurin[1], N.B. Skachkov[1,a]

Joint Institute for Nuclear Research, Dubna, Russia

Received: 17 June 2003 / Revised version: 8 July 2004 /
Published online: 24 August 2004 – © Springer-Verlag / Società Italiana di Fisica 2004

Abstract. The numbers of "γ+jet" events suitable for the determination of the gluon distribution function $f_g^p(x,Q^2)$ in a proton at the LHC for various intervals of x and Q^2 are estimated. The contributions of background events of different sources are studied and estimated in the considered intervals of x and Q^2. The PYTHIA event generator was used to produce physical events for this analysis.

1 Introduction

Modeling of the production processes of many new particles (Higgs boson, SUSY particles) in the forthcoming LHC experiments as well as the future physical analysis of the corresponding measurement are heavily based on the knowledge of the gluon distribution in a proton $f_g^p(x,Q^2)$ [1][1]. For this reason a study of the possibility of measuring the gluon density directly in the LHC experiments (especially in the kinematic region of small x and high Q^2) is of great interest.

One of the promising channels for this measurement is the inclusive prompt photon production [2]

$$pp \to \gamma^{\mathrm{dir}} + X. \tag{1}$$

The region of photon transverse momentum ${P_{\mathrm{t}}}^{\gamma}$, reached by the UA1 [3], UA2 [4], CDF [5] and D0 [6] experiments, extends up to ${P_{\mathrm{t}}}^{\gamma} \approx 60\,\mathrm{GeV}/c$ and, according to recent results [7], up to ${P_{\mathrm{t}}}^{\gamma} \approx 105\,\mathrm{GeV}/c$. These data together with the later ones [8–19] and the E706 [20], UA6 [21] results give, in principle, an opportunity for tuning the form of the gluon distribution [13,16,22,23]. The rates and an estimation of the cross sections of inclusive photon production at LHC are given in [2] (see also [24]).

Here we consider the process of the direct photon production in association with an opposite-side jet [12,13] (for experimental results, see [25–27])

$$pp \to \gamma^{\mathrm{dir}} + \mathrm{jet} + X. \tag{2}$$

In QCD leading order the processes (1) and (2) are caused by two subprocesses[2]: the "Compton-like" scattering

$$qg \to \gamma + q \tag{3}$$

and the "annihilation" subprocess

$$q\overline{q} \to \gamma + g. \tag{4}$$

The first one gives a dominant contribution to the cross sections of (1) and (2) [8,12,13] and serves as a "signal" subprocess due to its direct connection with the gluon distribution.

The study of the "γ+jet" process (2) is a more preferable one as compared with the inclusive direct photon production process (1) from the viewpoint of the extraction of information on the gluon distribution $f_g^p(x,Q^2)$[3]. First of all, this is explained by a higher value of the purity of the process (2) for which the signal-to-background (S/B) ratios are several times higher than the S/B ratios to the process (1) [30,33].

Secondly, while the cross section for the process (1) is given as an integral over the parton distribution functions (PDF) of a proton $f_a^p(x,Q^2)$, the cross section of the process (2) is expressed directly (at ${P_{\mathrm{t}}}^{\gamma} \geq 30\,\mathrm{GeV}/c$[4]) through these PDFs:

$$\frac{\mathrm{d}\sigma}{\mathrm{d}\eta_1 \mathrm{d}\eta_2 \mathrm{d}({P_{\mathrm{t}}^{\gamma}})^2} = \sum_{a,b} x_a\, f_a^p(x_a,Q^2)\, x_b\, f_b^p(x_b,Q^2) \frac{\mathrm{d}\sigma}{\mathrm{d}\hat{t}}(a\,b \to 1\,2), \tag{5}$$

[a] *Present address:* Joliot-Curie 6, JINR, 141980, Dubna, Moscow region, Russia

[1] For example, the production of the standard model Higgs boson is mainly caused by gluon–gluon fusion $gg \to H$ over the entire mass range [1].

[2] A contribution of another possible NLO channel $gg \to g\gamma$ was found to be still negligible even at LHC energies.

[3] A detailed study of "γ + jet" events and different aspects of their application can be found in [28,35].

[4] I.e. in the region where "k_{T} smearing effects" should not be important (for example, see [18]).

where $a, b = q, \bar{q}, g$; $1, 2 = q, \bar{q}, g, \gamma$. The incident parton momentum fractions x_a, x_b may be reconstructed from the final state photon and jet pseudorapidities $\eta_1 = \eta^{\gamma}$, $\eta_2 = \eta^{\rm jet}$ and $P_{\rm t}{}^{\gamma}$ according to the formula[5]

$$x_{a,b} = P_{\rm t}{}^{\gamma}/\sqrt{s} \cdot (\exp(\pm\eta_1) + \exp(\pm\eta_2)). \qquad (6)$$

Thus, (5) a knowledge of the experimentally determined triple cross section in the intervals of $\Delta\eta^{\gamma}$, $\Delta\eta^{\rm jet}$ and $(P_{\rm t}^{\gamma})^2$ with account of the results of the independent measurements of q, $\bar{q}$ distributions [31] allows the gluon distribution $f_g^p(x, Q^2)$ to be determined after a substantial reduction of the background contribution.

The $P_{\rm t}{}^{\gamma}$ distributions of the number of signal events remaining after application of strict selection criteria, proposed in [30,32], were presented earlier in [29,33,34][6].

Those selection criteria allow one to reduce considerably the background to the "$\gamma^{\rm dir} + {\rm jet}$" process (2) and select the events with a suppressed initial state radiation. Here we present a detailed study of the background fraction in different x and Q^2 intervals and show that the "gluonic" subprocess (3) gives a noticeable contribution to the total number of selected "$\gamma + {\rm jet}$" events [29].

This paper is organized as follows. The main background sources are discussed in Sect. 2. In Sect. 3 we list the selection criteria used to enhance the content of the signal events (3) in the selected data sample. In Sect. 4 the numbers of events suitable for an extraction of the gluon distribution function $f_g^p(x, Q^2)$ are estimated. The contribution of events of other types in different x and Q^2 intervals are also shown in this section. A possibility of further background events suppression by an account of the discrimination efficiencies between a single photon and π^0, η, ω and K_s^0 mesons as well as between quark and gluon jets is also demonstrated. Our conclusions follow in Sect. 5.

2 Background sources

The background to the events based on the process (2) is mainly caused by the following.

(1) The events with high $P_{\rm t}$ photons produced in the neutral decay channels of π^0, η, ω and K_s^0 mesons[7].

(2) The events with the photons radiated from a quark (i.e. bremsstrahlung photons) in the next-to-leading order QCD subprocesses of the $qg \to qg$, $qq \to qq$ and $q\bar{q} \to q\bar{q}$ scattering [30,33].

The background events of the first type will be called below the "γ–mes" events and the events of the second type "γ–brem" ones. More detailed information on the fundamental QCD subprocesses from which originate "γ–mes" and "γ–brem" events is presented in Sect. 4.

The background may be also caused by "$e^{\pm}$ events" which contain one jet and $e^{\pm}$ as a direct photon candidate. The value of the fraction of these events in the total background was estimated in [30,33] (see also Sects. 3 and 4).

The background containing the "γ–mes" events can be significantly suppressed by the event selection criteria, pointed out in [30,33]. It may be achieved, first of all, due to very strict photon isolation criteria because a parent meson (π^0, η, ω or K_s^0) is usually surrounded by other particles. Additional rejection factors were obtained from a full GEANT simulation of the physical processes in the CMS detector [38] where for the Barrel region ($|\eta| < 1.4$) we used information from the electromagnetic calorimeter (ECAL) cells only[8] [40] while for the Endcap region ($1.4 < |\eta| < 2.5$) the results of the analysis of hits in the preshower detector [41] were applied.

Especial attention should be paid to the events containing the bremsstrahlung photons. They are also noticeably rejected by the selection cuts but still constitute a significant part of the total background [30].

The simulation, performed with a help of the Monte Carlo event generator PYTHIA [42], has shown that in the selected "$\gamma + {\rm jet}$" event samples a large part of "γ–brem" events contains a gluon jet (see Sect. 4). For this part of the events, as well as for a part of "γ–mes" events with a gluon jet, one can take into consideration the quark/gluon separation efficiencies found earlier in [43]. The number of remaining background events also must be well estimated in order to subtract their contribution from the number of the selected "$\gamma^{\rm dir} + {\rm jet}$" events (2).

3 Definition of selection cuts

(1)[9] We consider only the events with one jet and one "$\gamma^{\rm dir}$-candidate" (in what follows we shall denote this also as $\tilde{\gamma}$ and call this "photon" for brevity) with

$$P_{\rm t}{}^{\rm jet} \geq 30\,{\rm GeV}/c \quad \text{and} \quad P_{\rm t}{}^{\tilde{\gamma}} \geq 40\,{\rm GeV}/c. \qquad (7)$$

In the simulation the signal (most energetic γ or $e^{\pm}$ together with surrounding particles) is considered as a candidate for a direct photon if it fits into one CMS calorimeter tower having the size of 0.087×0.087 in the η–ϕ space [38].

For all applications a jet is defined according to the PYTHIA jetfinding simple cone algorithm LUCELL [42]. In the η–ϕ space the jet cone of radius R counted from the jet initiator cell is taken to be $R = ((\Delta\eta)^2 + (\Delta\phi)^2)^{1/2} = 0.7$.

[5] See, for instance, [11,12].

[6] Analogous estimations for the Tevatron were done in [35, 36].

[7] As it was shown in [37] the charged decay channels of those mesons can be strongly suppressed even without tracker information.

[8] A preshower detector is not foreseen currently in the Barrel region of the CMS detector [38].

[9] In this section we follow mostly the selection criteria from [30,32,33].

(2) To suppress the contribution of background processes, i.e. to select mostly the events with the "isolated" photons and to discard the events that fake a direct photon signal, we restrict:

(a) the value of the scalar sum of P_t of hadrons and other particles surrounding a photon within a cone of $R^{\gamma}_{\rm isol} = ((\Delta\eta)^2 + (\Delta\phi)^2)^{1/2} = 0.7$ ("absolute isolation cut")

$$\sum_{i \in R_{\rm isol}} {P_{\rm t}}^{i} \equiv {P_{\rm t}}^{\rm isol} \leq P_{\rm t\,CUT}^{\rm isol}; \tag{8}$$

(b) the value of a fraction ("fractional isolation cut")

$$\sum_{i \in R_{\rm isol}} {P_{\rm t}}^{i} / {P_{\rm t}}^{\tilde{\gamma}} \equiv \epsilon^{\gamma} \leq \epsilon^{\gamma}_{\rm CUT}. \tag{9}$$

(3) Only the events having no tracks[10] with $P_t > 1\,\mathrm{GeV}/c$ contained inside the cone of $R = 0.4$ around a $\gamma^{\rm dir}$-candidate are accepted.

(4) To suppress the background events with photons resulting from π^0, η, ω and K^0_S meson decays, we require the absence of a high P_t hadron in the tower containing the $\gamma^{\rm dir}$-candidate:

$${P_{\rm t}}^{\rm hadr} \leq 7\,\mathrm{GeV}/c. \tag{10}$$

At the PYTHIA level of simulation this cut may effectively take into account the imposing of an upper cut on the energy deposited in the cells of the hadronic calorimeters (HCAL) that are behind the ECAL signal cells fired by the photon [37].

In real experimental conditions one can require the fraction of the photon energy deposited in ECAL to be greater than some threshold[11].

(5) We select the events with the vector ${\mathbf{P}_{\rm t}}^{\rm jet}$ being "back-to-back" to the vector ${\mathbf{P}_{\rm t}}^{\tilde{\gamma}}$ (in the plane transverse to the beam line) within the azimuthal angle interval $\Delta\phi$ defined by

$$\phi_{(\gamma,\rm jet)} = 180^{\circ} \pm \Delta\phi. \tag{11}$$

The angle $\phi_{(\gamma,\rm jet)}$ between the ${\mathbf{P}_{\rm t}}^{\tilde{\gamma}}$ and ${\mathbf{P}_{\rm t}}^{\rm jet}$ vectors is calculated from the expression ${\mathbf{P}_{\rm t}}^{\tilde{\gamma}}{\mathbf{P}_{\rm t}}^{\rm jet} = {P_{\rm t}}^{\tilde{\gamma}}{P_{\rm t}}^{\rm jet}\cos(\phi_{(\gamma,\rm jet)})$ with ${P_{\rm t}}^{\tilde{\gamma}} = |{\mathbf{P}_{\rm t}}^{\tilde{\gamma}}|$ and ${P_{\rm t}}^{\rm jet} = |{\mathbf{P}_{\rm t}}^{\rm jet}|$. The value of $\Delta\phi$ may be chosen from the interval $5^{\circ} \div 15^{\circ}$ for various energies.

(6) We also choose only the events that do not have any other, except one jet, minijet (or cluster) high P_t activity with the ${P_{\rm t}}^{\rm clust}$ higher than some threshold $P_{\rm t\,CUT}^{\rm clust}$ value. Thus, we select events with

$${P_{\rm t}}^{\rm clust} \leq P_{\rm t\,CUT}^{\rm clust}, \tag{12}$$

where clusters are found by the same jetfinder LUCELL used to determine the main jet in the event. The most effective restrictions are $P_{\rm t\,CUT}^{\rm clust} = 5 \div 15\,\mathrm{GeV}/c$. Their choice will be caused mostly by the gained statistics and ${P_{\rm t}}^{\tilde{\gamma}}$ value (for higher ${P_{\rm t}}^{\tilde{\gamma}}$ a weaker $P_{\rm t\,CUT}^{\rm clust}$ can be used).

(7) The events containing $e^{\pm}$ as a photon candidate are mainly caused by the subprocesses $q\,g \to q' + W^{\pm}$ and $q\,\bar{q}' \to g + W^{\pm}$ with the subsequent decay $W^{\pm} \to e^{\pm}\nu$. To reduce a contribution from these events [30,33] we shall select only events having a small value of missing transverse momentum ${P_{\rm t}}^{\rm miss}$. So, we also use the following cut:

$${P_{\rm t}}^{\rm miss} \leq P_{\rm t\,CUT}^{\rm miss}. \tag{13}$$

Finally, in what follows we shall set the values of the cut parameters (besides those pointed out above explicitly) as specified below:

$$\begin{aligned} &P_{\rm t\,CUT}^{\rm isol} = 2\,\mathrm{GeV}/c,\ \ \epsilon^{\gamma}_{\rm CUT} = 5\%,\ \ \Delta\phi \leq 15^{\circ}, \\ &P_{\rm t\,CUT}^{\rm clust} = 10\,\mathrm{GeV}/c,\ \ P_{\rm t\,CUT}^{\rm miss} = 10\,\mathrm{GeV}/c. \end{aligned} \tag{14}$$

4 Determining the numbers of events and reducing the background

To estimate a background to the signal events we have done a simulation using the Monte Carlo event generator PYTHIA with a mixture of all existing in PYTHIA QCD and SM subprocesses with large cross sections[12], including the subprocesses (3) and (4)[13].

The total cross section of the background subprocesses exceeds the cross section of the subprocesses (3) and (4) by more than three orders of magnitude. The GRV 94L parameterization of the parton distribution functions is used as the default one.

Five generations (each of about 60 to 90 million events) with different values of minimal transverse momentum of a hard subprocess[14] $\hat{p}_{\perp}^{\rm min}$ were done to cover six ${P_{\rm t}}^{\gamma}$ intervals: $\hat{p}_{\perp}^{\rm min} = 40$ (for $40 < {P_{\rm t}}^{\gamma} < 71$), 70 (for $71 < {P_{\rm t}}^{\gamma} < 100$), 100 (for $100 < {P_{\rm t}}^{\gamma} < 141$), 140 (for $141 < {P_{\rm t}}^{\gamma} < 200$) and 200 (for $200 < {P_{\rm t}}^{\gamma} < 283\,\mathrm{GeV}/c$. The values of the other main physical parameters are taken by default [42]. The cross sections of the abovementioned subprocesses define the rates of the corresponding physical events and, thus, appear here as weight factors. The selection criteria of Sect. 3 were applied then to the generated events.

The total numbers of these events, i.e. events originating from the subprocesses (3) and (4) as well as "γ–brem" and "γ–mes" events, are presented (being divided by the factor of 10^3) in Table 1 for each x and Q^2 interval ($Q^2 \equiv ({P_{\rm t}}^{\gamma})^2$) for the integrated luminosity[15] $L_{\rm int} = 10\,\mathrm{fb}^{-1}$. The momentum fractions x_a and x_b of the

[10] I.e. charged particles as we use the PYTHIA level of simulation.

[11] E.g. to be greater than 0.96 (as it was used at D0 [7]).

[12] They have ISUB = 11–20, 28–31, 53, 68 according to the process numbers in PYTHIA [42].

[13] With ISUB = 14 and 29 in the notation of PYTHIA [42].

[14] The CKIN(3) parameter in PYTHIA.

[15] This value is intended to be accumulated during one year of LHC running at a luminosity of $L = 10^{33}\,\mathrm{cm}^{-2}\,\mathrm{s}^{-1}$.

Table 1. Numbers of all events (divided by 10^3) in Q^2 and x intervals for $L_{\rm int} = 10\,{\rm fb}^{-1}$

Q^2	x values of a parton				All x	$P_{\rm t}{}^{\gamma}$
$({\rm GeV}/c)^2$	10^{-4}–10^{-3}	10^{-3}–10^{-2}	10^{-2}–10^{-1}	10^{-1}–10^{0}	10^{-4}–10^{0}	(GeV/c)
1600–2500	1393.6	4301.1	4506.8	481.4	10682.9	40–50
2500–5000	561.1	2931.0	3174.7	430.4	7097.2	50–71
5000–10000	61.7	665.6	769.6	196.1	1693.0	71–100
10000–20000	3.6	150.3	178.4	81.7	414.0	100–141
20000–40000	0.0	29.9	40.9	25.2	96.0	141–200
40000–80000	0.0	5.7	10.7	7.8	24.2	200–283
					20 007.3	

initial state partons were calculated via the photon and jet parameters according to (6). The right-hand columns of this table show, for convenience, the correspondence of the Q^2 interval to the $P_{\rm t}{}^{\gamma}$ interval.

One can see from Table 1 that at $40 < P_{\rm t}{}^{\gamma} < 50\,{\rm GeV}/c$ the total number of events is about 10 million and it drops to 24 200 at $200 < P_{\rm t}{}^{\gamma} < 283\,{\rm GeV}/c$, i.e. with five-fold increase of $P_{\rm t}{}^{\tilde{\gamma}}$ the spectrum drops by about 400 times.

The contribution from the background "$e^{\pm}$ events" was not included in Table 1. The number of these type events was estimated in [30,33][16] and found to be very small as compared with other background types. Thus, in what follows we shall concentrate on a more sizable background.

Now let us look at the contributions of different event types in various x and Q^2 intervals. The events selected after passing the criteria of Sect. 3 were classified in accordance with the origin of the produced $\gamma^{\rm dir}$-candidates. So we consider separately those that contain the direct photons (produced in the subprocesses (3) and (4)) and those that have $\gamma^{\rm dir}$-candidates appearing due to the radiation from quarks ("γ–brem" events) or from the π^0, η, ω and K_s^0 meson decays ("γ–mes" events). All these contributions are presented in Tables 1A–4A of the appendix in the form of the number of events divided by factor of 10^3. The numbers of events based on the Compton (3) and annihilation (4) subprocesses are shown in Tables 1A and 2A while the numbers of the "γ–brem" and "γ–mes" events can be found in Tables 3A and 4A, respectively.

These numbers were obtained after passing the selection criteria of Sect. 3. The fractions of each event type, calculated for a given interval of $P_{\rm t}{}^{\tilde{\gamma}}$, are presented in Fig. 1a (100% is taken for all types of events).

We see that the main part of the background is due to "γ–brem" events and the combined contribution of "γ–brem" and "γ–mes" events into the total number of events varies from about 23% at $40 < P_{\rm t}{}^{\tilde{\gamma}} < 50\,{\rm GeV}/c$ to about 6% at $100 < P_{\rm t}{}^{\tilde{\gamma}} < 140\,{\rm GeV}/c$ and drops to 4% at $200 < P_{\rm t}{}^{\tilde{\gamma}} < 283\,{\rm GeV}/c$.

We would like to stress that the essential point of our analysis is the study of the background contributions after application of the cuts for selecting the "γ + jet" events

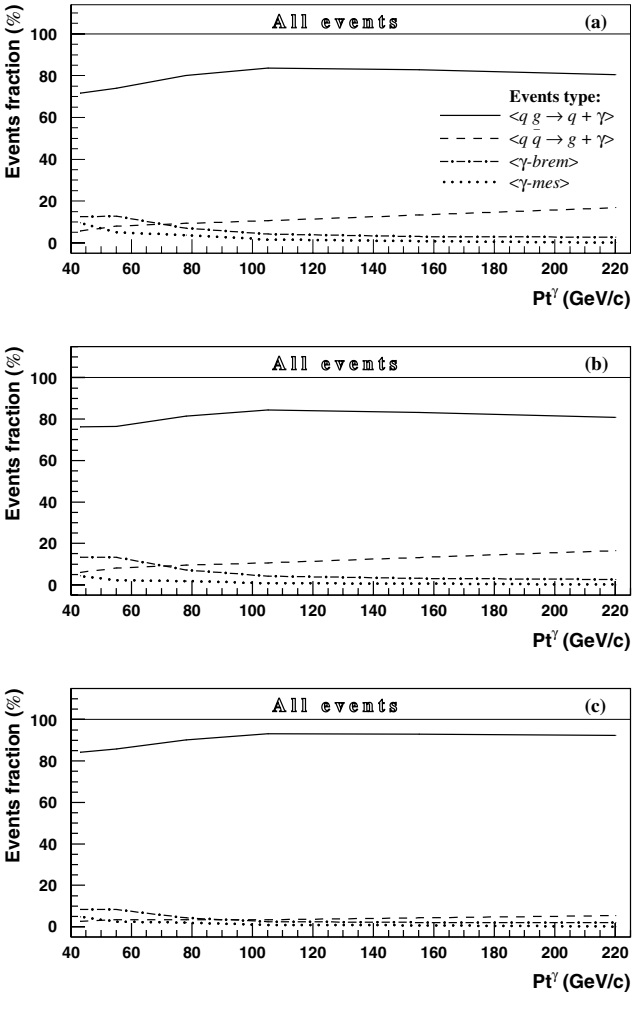

Fig. 1. The contributions of various events types to the total number of events as a function of $P_{\rm t}{}^{\tilde{\gamma}}$ presented for three cases. **a** No separation efficiency is taken into account, **b** the separation efficiencies $\epsilon^{\gamma/{\rm mes}}$ are taken into account and **c** the separation efficiencies $\epsilon^{\gamma/{\rm mes}}$ and $\epsilon^{q/g}$ are taken into account

[16] It was found that after application of the selection criteria from Sect. 3 and taking the track finding efficiency to be equal to 85% (being averaged over all pseudorapidity range) [39] a contribution of the $e^{\pm}$ events (having the isolated $e^{\pm}$ with $P_{\rm t}{}^{e} > 40\,{\rm GeV}/c$) to the total background reduces to less than 1% at $40 \le P_{\rm t}{}^{e} \le 70\,{\rm GeV}/c$ and to about 5% at $P_{\rm t}{}^{e} \ge 100\,{\rm GeV}/c$.

Table 2. Numbers of all events (divided by 10^3) in Q^2 and x intervals for $L_{\rm int} = 10\,{\rm fb}^{-1}$. The separation efficiencies $\epsilon^{\gamma/{\rm mes}}$ are taken into account

Q^2	x values of a parton				All x	$P_{\rm t}{}^{\gamma}$
$({\rm GeV}/c)^2$	10^{-4}–10^{-3}	10^{-3}–10^{-2}	10^{-2}–10^{-1}	10^{-1}–10^{0}	10^{-4}–10^{0}	(GeV/c)
1600–2500	1214.6	3073.1	3433.1	394.5	8115.4	40–50
2500-5000	502.8	2220.7	2478.2	364.0	5565.8	50–71
5000-10000	54.1	532.8	587.8	168.7	1343.7	71–100
10000–20000	3.2	124.4	134.6	70.6	333.1	100–141
20000–40000	0.0	25.3	30.1	21.8	77.3	141–200
40000–80000	0.0	4.9	7.9	6.6	19.4	200–283
					15 454.7	

with a limited cluster/minijet activity and a clean γ–jet topology.

Only in this case a contribution of "γ–brem" and "γ–mes" events can be decreased noticeably[17].

The selection criteria of Sect. 3 are not final and are moderate enough. The results of their application may change if we vary some cuts. So, for example, a stronger limitation of the cluster activity (12) by $P_{\rm t\,CUT}^{\rm clust} = 5\,{\rm GeV}/c$ would lead to a further substantial decreasing of the numbers of "γ–brem" and "γ–mes" events [30].

The contribution of "γ–mes" events can also be reduced by the account of the difference between a single photon and the π^0, η, ω and K_s^0 meson signals produced in the detector.

To take into account the discrimination efficiencies between a single photon and the photons produced via multiphoton decays of π^0, η, ω and K_s^0 mesons ($\epsilon^{\gamma/{\rm mes}}$), the results of [40,41] were used. The efficiencies found in [40] were obtained by the analysis of the ECAL crystal cells only in the Barrel region ($|\eta| < 1.4$) while the efficiencies in [41] are found from the analysis of hits in the preshower detector in the Endcap region ($1.4 < |\eta| < 2.5$). The results of [40,41] are briefly the following: the rejection efficiency of the neutral pion is about 49–67% (depending on the energy) in the Barrel region and it ranges in 45–71% for the Endcap region. The single photon selection efficiencies ($\epsilon_{\rm sel}^{\gamma}$) were set to 70% and 91% in the first and second cases respectively[18].

The results of the applications of the γ/meson separation efficiencies described above to the "γ–mes" events themselves are placed in Table 8A (compare with Table 4A) and in Tables 5A–7A of the appendix for other event types.

Thus, we see that for the "γ–mes" events the reduction factor of about 2–3 for $40 < P_{\rm t}{}^{\tilde{\gamma}} < 100\,{\rm GeV}/c$ can be obtained with a loss of 16–19% of events of other types with a single photon in the final state. The total numbers of all events left after account of the separation efficiencies $\epsilon^{\gamma/{\rm mes}}$ are presented in Table 2.

The physical models implemented in PYTHIA allows one to get an idea about the possible origin of the "γ–brem" and "γ–mes" events. Tables 3 and 4 show the relative contributions of the four main (having the largest cross sections) fundamental QCD subprocesses, $qg \to qg$, $qq \to qq$, $gg \to q\bar{q}$ and $gg \to gg$, into a production of the "γ–brem" and "γ–mes" events selected with the criteria 1–7 of Sect. 3 for three $P_{\rm t}{}^{\tilde{\gamma}}$ intervals[19].

One can see from these tables that most of the "γ–brem" and "γ–mes" events (from 70 to 80%) still originate from "gluonic" $qg \to qg$, $gg \to q\bar{q}$ and $gg \to gg$ subprocesses with a dominant contribution from the first subprocess.

The analysis of the PYTHIA simulation output also shows that practically in all of the selected "γ–brem" events the bremsstrahlung photons are produced in the final state of the fundamental subprocess. They are radiated from the outgoing quarks in the case of the first three subprocesses or can appear as the result of string breaking in the case of $gg \to gg$ scattering. The last mechanism, naturally, gives a small contribution into the "γ–brem" events production. In the first case the selected (see Sect. 3) photon carries away almost all energy of a quark in the final state. The events of this kind have mostly a

[17] It was shown in [30] that, for instance, at $P_{\rm t}{}^{\gamma} > 100\,{\rm GeV}/c$, the application of "photonic" cuts, usually used to select inclusive photon "$\gamma + X$" events, gives $S/B = 1.9$ only, while a further account of "hadronic" and topological cuts for selection of "γ + jet" events leads to $S/B = 17.6$, i.e. *to the increase of S/B by about one order of magnitude* (here S is a total contribution from the events based on the subprocesses (3) and (4) and B is the contribution from the sum of "γ–brem" and "γ–mes" events). The application of other cuts that limit the $P_{\rm t}$ activity out of the "γ + jet" system may lead to the following 20–30% increase of the S/B ratio [30].

[18] With the same $\epsilon_{\rm sel}^{\gamma} = 70\%$ one can also reject about 90–95% of the "η–meson events" and 55–92% of the "K_s^0–meson events" [40] in the Barrel region. For the Endcap the respective rejection efficiencies were taken here equal to those obtained for the π^0 meson. At the same time it is worth to note that the main contribution to the "γ–mes" background comes from the "π^0-events" ($\sim$ 62–65% in the interval $40 < P_{\rm t}{}^{\tilde{\gamma}} < 140\,{\rm GeV}/c$) [30,33].

[19] The sum over contributions from the four considered QCD subprocesses in some lines of Tables 3 and 4 is less than 100%. The remaining percentages correspond to other subprocesses (like $q\bar{q} \to q\bar{q}$ or $qg \to q'W^{\pm}$). The errors in those tables are statistical and caused by the number of entries for various background types after application of the criteria 1–7 of Sect. 3.

Table 3. Relative contribution (in per cents) of main QCD subprocesses into the "γ–brem" events production

$P_t^{\tilde{\gamma}}$	fundamental QCD subprocess			
(GeV/c)	$qg \to qg$	$qq \to qq$	$gg \to q\bar{q}$	$gg \to gg$
40–71	70.6 ± 8.7	21.1 ± 3.8	5.1 ± 1.6	2.6 ± 1.0
71–141	67.5 ± 7.3	23.6 ± 3.5	4.2 ± 1.2	2.6 ± 0.9
141–283	58.7 ± 9.0	30.7 ± 5.7	1.8 ± 1.0	–

Table 4. Relative contribution (in per cents) of main QCD subprocesses into the "γ–mes" events production

$P_t^{\tilde{\gamma}}$	fundamental QCD subprocess			
(GeV/c)	$qg \to qg$	$qq \to qq$	$gg \to q\bar{q}$	$gg \to gg$
40–71	65.2 ± 9.9	20.1 ± 4.5	7.1 ± 2.5	7.2 ± 2.3
71–141	63.7 ± 11.6	23.0 ± 5.2	7.2 ± 2.6	4.4 ± 1.4
141–283	57.7 ± 26.2	23.1 ± 13.9	7.7 ± 6.9	3.8 ± 4.6

Table 5. Numbers of all events (divided by 10^3) in Q^2 and x intervals for $L_{\rm int} = 10\,{\rm fb}^{-1}$. The separation efficiencies $\epsilon^{\gamma/{\rm mes}}$ and $\epsilon^{q/g}$ are taken into account

Q^2	x values of a parton				All x	P_t^{γ}
(GeV/c)^2	10^{-4}–10^{-3}	10^{-3}–10^{-2}	10^{-2}–10^{-1}	10^{-1}–10^{0}	10^{-4}–10^{0}	(GeV/c)
1600–2500	721.3	1858.7	2052.9	217.6	4850.5	40–50
2500–5000	302.3	1314.1	1449.4	206.2	3271.9	50–71
5000–10000	31.5	320.0	350.0	99.9	801.5	71–100
10000–20000	1.9	74.4	81.1	41.8	199.1	100–141
20000–40000	0.0	14.9	18.2	12.6	45.6	141–200
40000–80000	0.0	2.9	4.5	3.8	11.2	200–283
					9 179.8	

gluon jet (70.6% of events for $40 < P_t^{\tilde{\gamma}} < 71\,{\rm GeV}/c$ interval and 58.7% of events for $141 < P_t^{\tilde{\gamma}} < 283\,{\rm GeV}/c$) with the photon radiated in the back-to-back direction to the jet in the ϕ plane. In the second case ($gg \to gg$ based events) a remaining jet is practically always of the gluon type.

As for "γ–mes" events, it is natural to expect that in the events based on the $qg \to qg$ scattering after suppression of the cluster activity by the cut $P_t^{\rm clust} < 10\,{\rm GeV}/c$ (see (12)) a remaining jet can originate with an equal probability from a quark as well as from a gluon (50% by 50%) while in the events based on the $qq \to qq$, $gg \to q\bar{q}$ ($gg \to gg$) subprocesses the jet is always of the quark (gluon) type.

Thus, one can conclude that about 73% (40%), 70% (36%) and 59% (33%) of the "γ–brem" ("γ–mes") events have a gluon jet in the selected one-jet events in the $P_t^{\tilde{\gamma}}$ intervals $40 \div 71$, $71 \div 141$ and $141 \div 283\,{\rm GeV}/c$, respectively.

For the following suppression of the contributions from "γ–brem" and "γ–mes" events having a gluon jet in the final state one can apply the quark/gluon separation efficiencies ($\epsilon^{q/g}$) obtained earlier in [43]. The results of [43] show that with a quark jet selection efficiency of about 65–67% it is possible to reject 73–81% of the gluons jets[20] for $P_t^{\rm jet}$ varying from 40 to $200\,{\rm GeV}/c$.

The numbers of different types of events after taking into account both the $\epsilon^{\gamma/{\rm mes}}$ and $\epsilon^{q/g}$ separation efficiencies are presented in Tables 9A–12A of the appendix while their fractions (in %) are shown in Fig. 1c.

By comparing Tables 7A and 11A one can see that the numbers of "γ–brem" events[21] are reduced by 2.5–3 times at the cost of 35% loss of the events based on the subprocess (3) and their fraction in the total number of events becomes about 8% at $40 < P_t^{\tilde{\gamma}} < 50\,{\rm GeV}/c$ and about 2% at $140 < P_t^{\tilde{\gamma}} < 200\,{\rm GeV}/c$. *The total contributions of the "γ–brem" and "γ–mes" events in the same $P_t^{\tilde{\gamma}}$ intervals are* 13.2% *and* 2.8%*, respectively.*

We see also that the account of $\epsilon^{q/g}$, the separation efficiency, reduces the contribution of the events originating from the annihilation subprocess (4) to the total number of events (especially at higher P_t^{γ}) to a size of about 3–5% over the whole considered P_t^{γ} range (see Fig. 1 and Tables 1A–8A).

The final numbers of all "γ + jet" events for the luminosity $L_{\rm int} = 10\,{\rm fb}^{-1}$ at different x and Q^2 intervals after taking into account both separation efficiencies are given in Table 5. We see that after passing all selection cuts and application of the efficiencies $\epsilon^{\gamma/{\rm mes}}$ and $\epsilon^{q/g}$ one can get about 5 million events at the $40 < P_t^{\tilde{\gamma}} < 50\,{\rm GeV}/c$ interval, about 200 000 at $100 < P_t^{\tilde{\gamma}} < 141\,{\rm GeV}/c$ and about 11 000 at the last considered interval of $200 < P_t^{\tilde{\gamma}} < 283\,{\rm GeV}/c$. *The total expected statistics on the "γ + jet" events, left after taking into account the $\epsilon^{\gamma/{\rm mes}}$ and $\epsilon^{q/g}$ efficiencies, is about* $9 \cdot 10^6$ *events.* The final contributions of different subprocesses in various x and Q^2 intervals are presented in Tables 9A–12A.

[20] This efficiency slightly depends on the jet transverse momentum $P_t^{\rm jet}$ and pseudorapidity $\eta^{\rm jet}$ [43].

[21] These are, in fact, irreducible by using only photon information after application of the strong isolation cuts (8) and (9).

5 Conclusions

The results presented above show that during one year of LHC running at low luminosity ($L = 10^{33}\,\mathrm{cm}^{-2}\,\mathrm{s}^{-1}$) one can collect after application of the proposed selection criteria a clean sample of "$\gamma^{\mathrm{dir}}+\mathrm{jet}$" events with a sufficient statistics to determine the gluon density in a proton in the new kinematic region of $2\cdot10^{-4} \le x \le 1$ and $1.6\cdot10^{3} \le Q^2 \le 2\cdot10^{5}\,(\mathrm{GeV}/c)^2$. At the same time the combined contribution of "γ–brem" events and "γ–mes" events is estimated to be about 23% at $40 < P_{\mathrm{t}}{}^{\tilde{\gamma}} < 50\,\mathrm{GeV}/c$ and it drops to 4% at $200 < P_{\mathrm{t}}{}^{\tilde{\gamma}} < 283\,\mathrm{GeV}/c$ (see Tables 1A–4A and Fig. 1a).

The given estimations for the contributions of the "γ–brem" and "γ–mes" events are not final yet. For instance, a stronger limitation of $P_{\mathrm{tCUT}}^{\mathrm{clust}} = 5\,\mathrm{GeV}/c$ (12) would lead to the following substantial (about 30%) reduction of their contribution [30].

With an additional account of the discrimination efficiencies between single photons and π^0, η, K_s^0 mesons as well as those between quark and gluon jets [40,41,43] one can increase noticeably the purity of the selected samples of the "$\gamma^{\mathrm{dir}}+\mathrm{jet}$" events (see Tables 9A–12A of the appendix and Fig. 1). A possibility to obtain better background rejection factors will depend on the chosen values of the single photon and quark jet selection efficiencies[22] which in their turn will be caused by a gained statistics of the "$\gamma+\mathrm{jet}$" events.

It is also worth mentioning that a full simulation[23] of the signal and background processes is rather difficult due to the very small selection efficiency for the background events ($\approx$ 0.01–0.05% depending on the energy) [28,30] which, in its turn, requires huge computational resources to collect the background events statistics sufficient for the analysis.

Figure 2 shows in the widely used (x, Q^2) kinematic plot (see also [44]) what area can be covered for studying the process $qg \to \gamma + q$. From this figure (and Tables 1, 2, 5) it becomes clear that even at low LHC luminosity it would be possible to study the gluon distribution with a good statistics of "γ+jet" events in the region of small x at values of Q^2 that are about 2 orders of magnitude higher than those reached at HERA now. It is worth emphasizing that an extension of the experimentally reachable region at LHC to the region of lower values of Q^2 to obtain more overlapping with the area covered by HERA would also be of great interest.

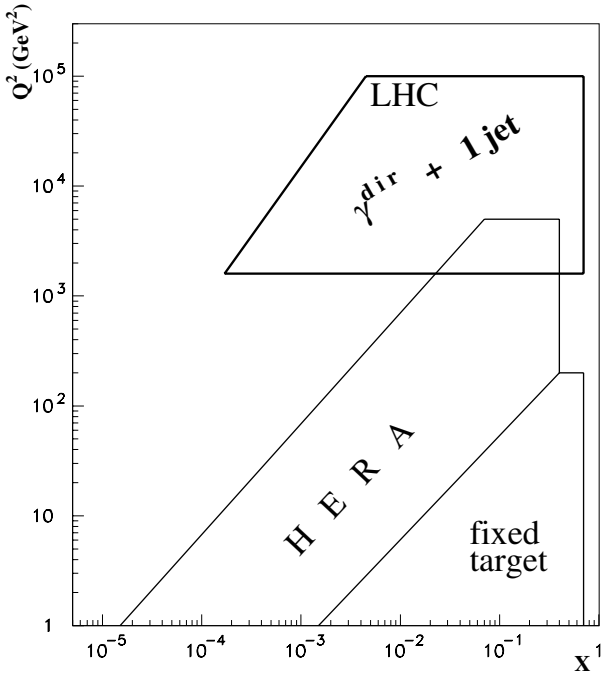

Fig. 2. LHC (x, Q^2) kinematic region for the $pp \to \gamma + \mathrm{jet}$ process

Acknowledgements. We are greatly thankful to D. Denegri, who stimulated us to study the physics of "γ + jet" processes, for permanent support and fruitful suggestions. It is a pleasure for us to express our recognition for helpful discussions to P. Aurenche, M. Dittmar, M. Fontannaz, J.Ph. Guillet, M.L. Mangano, E. Pilon, H. Rohringer, S. Tapprogge, H. Weerts and J. Womersley.

Appendix

Table 1A. Numbers of "$qg \to q + \gamma$" events (divided by 10^3) in Q^2 and x intervals at $L_{\mathrm{int}} = 10\,\mathrm{fb}^{-1}$

Q^2	x values of a parton				All x
$(\mathrm{GeV}/c)^2$	10^{-4}–10^{-3}	10^{-3}–10^{-2}	10^{-2}–10^{-1}	10^{-1}–10^{0}	10^{-4}–10^{0}
1600–2500	1040.3	3128.7	3202.5	275.6	7647.1
2500–5000	451.2	2185.8	2326.8	280.8	5244.6
5000–10000	45.4	545.5	611.8	151.6	1354.4
10000–20000	2.9	125.5	151.1	66.7	346.2
20000–40000	0	24.6	35.2	19.9	79.6
40000–80000	0	4.7	8.5	6.2	19.4

[22] Let us recall that the single photon selection efficiencies equal 70% and 91% for the Barrel and Endcap regions and quark jet selection efficiencies equal to about 65% were chosen here for the given estimations.

[23] We mean a full simulation of the detector response with the following digitization and reconstruction of signals from physical objects.

Table 2A. Numbers of "$q\bar{q} \to \gamma + g$" events (divided by 10^3) in Q^2 and x intervals at $L_{\text{int}} = 10\,\text{fb}^{-1}$

Q^2	x values of a parton				All x
$(\text{GeV}/c)^2$	10^{-4}–10^{-3}	10^{-3}–10^{-2}	10^{-2}–10^{-1}	10^{-1}–10^{0}	10^{-4}–10^{0}
1600–2500	120.3	190.2	236.8	50.5	597.8
2500–5000	43.1	239.7	250.1	35.3	568.2
5000–10000	7.7	60.5	69.0	20.5	157.7
10000–20000	0.7	16.9	15.9	10.3	43.8
20000–40000	0	4.2	4.4	4.2	12.8
40000–80000	0	0.9	1.8	1.4	4.1

Table 3A. Numbers of "γ–brem" events (divided by 10^3) in Q^2 and x intervals at $L_{\text{int}} = 10\,\text{fb}^{-1}$

Q^2	x values of a parton				All x
$(\text{GeV}/c)^2$	10^{-4}–10^{-3}	10^{-3}–10^{-2}	10^{-2}–10^{-1}	10^{-1}–10^{0}	10^{-4}–10^{0}
1600–2500	143.6	508.5	578.3	104.8	1335.3
2500–5000	51.3	328.2	432.1	94.8	906.5
5000–10000	4.3	42.0	59.0	13.7	119.0
10000–20000	0	5.2	9.2	2.8	17.2
20000–40000	0	0.9	0.9	1.0	2.8
40000–80000	0	0.1	0.4	0.2	0.7

Table 4A. Numbers of "γ–mes" events (divided by 10^3) in Q^2 and x intervals at $L_{\text{int}} = 10\,\text{fb}^{-1}$

Q^2	x values of a parton				All x
$(\text{GeV}/c)^2$	10^{-4}–10^{-3}	10^{-3}–10^{-2}	10^{-2}–10^{-1}	10^{-1}–10^{0}	10^{-4}–10^{0}
1600–2500	89.3	473.6	489.1	50.5	1102.4
2500–5000	15.5	177.3	165.6	19.4	377.7
5000–10000	4.3	17.6	29.5	10.3	61.6
10000–20000	0	2.6	2.2	1.9	6.7
20000–40000	0	0.2	0.4	0.2	0.8
40000–80000	0	0	0.02	0.01	0.03

Table 5A. Numbers of "$qg \to q + \gamma$" events (divided by 10^3) in Q^2 and x intervals at $L_{\text{int}} = 10\,\text{fb}^{-1}$. The separation efficiencies $\epsilon^{\gamma/\text{mes}}$ are taken into account

Q^2	x values of a parton				All x
$(\text{GeV}/c)^2$	10^{-4}–10^{-3}	10^{-3}–10^{-2}	10^{-2}–10^{-1}	10^{-1}–10^{0}	10^{-4}–10^{0}
1600–2500	945.0	2387.4	2608.6	246.7	6187.8
2500–5000	410.5	1723.1	1865.0	253.0	4251.7
5000–10000	41.3	443.2	475.5	134.6	1094.6
10000–20000	2.6	105.0	114.5	58.7	281.0
20000–40000	0	20.9	25.9	17.3	64.2
40000–80000	0	4.0	6.3	5.3	15.7

Table 6A. Numbers of "$q\bar{q} \to \gamma + g$" events (divided by 10^3) in Q^2 and x intervals at $L_{\rm int} = 10\,{\rm fb}^{-1}$. The separation efficiencies $\epsilon^{\gamma/{\rm mes}}$ are taken into account

Q^2	x values of a parton				All x
$({\rm GeV}/c)^2$	10^{-4}–10^{-3}	10^{-3}–10^{-2}	10^{-2}–10^{-1}	10^{-1}–10^{0}	10^{-4}–10^{0}
1600–2500	109.5	142.9	192.6	451.0	490.2
2500–5000	39.2	185.1	196.8	29.7	451.0
5000–10000	7.0	48.7	54.1	17.9	127.8
10000–20000	0.6	13.8	12.1	8.8	35.4
20000–40000	0	3.5	3.2	3.5	10.2
40000–80000	0	0.7	1.3	1.1	3.2

Table 7A. Numbers of "γ–brem" events (divided by 10^3) in Q^2 and x intervals at $L_{\rm int} = 10\,{\rm fb}^{-1}$. The separation efficiencies $\epsilon^{\gamma/{\rm mes}}$ are taken into account

Q^2	x values of a parton				All x
$({\rm GeV}/c)^2$	10^{-4}–10^{-3}	10^{-3}–10^{-2}	10^{-2}–10^{-1}	10^{-1}–10^{0}	10^{-4}–10^{0}
1600–2500	129.9	394.3	476.6	87.2	1088.0
2500–5000	46.7	258.5	359.8	74.8	739.8
5000–10000	3.9	34.0	47.1	11.7	96.6
10000–20000	0	4.4	7.1	2.4	13.9
20000–40000	0	0.8	0.7	0.9	2.4
40000–80000	0	0.1	0.3	0.2	0.6

Table 8A. Numbers of "γ–mes" events (divided by 10^3) in Q^2 and x intervals at $L_{\rm int} = 10\,{\rm fb}^{-1}$. The separation efficiencies $\epsilon^{\gamma/{\rm mes}}$ are taken into account

Q^2	x values of a parton				All x
$({\rm GeV}/c)^2$	10^{-4}–10^{-3}	10^{-3}–10^{-2}	10^{-2}–10^{-1}	10^{-1}–10^{0}	10^{-4}–10^{0}
1600–2500	30.2	148.5	155.2	15.4	349.4
2500–5000	6.4	53.9	56.6	6.4	123.3
5000–10000	1.9	6.9	11.2	4.6	24.6
10000–20000	0	1.1	0.9	0.8	2.8
20000–40000	0	0.1	0.3	0.1	0.5
40000–80000	0	0	0.01	0.01	0.02

Table 9A. Numbers of "$qg \to q + \gamma$" events (divided by 10^3) in Q^2 and x intervals at $L_{\rm int} = 10\,{\rm fb}^{-1}$. The separation efficiencies $\epsilon^{\gamma/{\rm mes}}$ and $\epsilon^{q/g}$ are taken into account

Q^2	x values of a parton				All x
$({\rm GeV}/c)^2$	10^{-4}–10^{-3}	10^{-3}–10^{-2}	10^{-2}–10^{-1}	10^{-1}–10^{0}	10^{-4}–10^{0}
1600–2500	623.7	1575.7	1721.7	162.8	4084.0
2500–5000	271.0	1137.3	1230.9	167.0	2806.2
5000–10000	27.3	292.5	313.8	88.9	722.5
10000–20000	1.7	69.4	75.6	38.7	185.5
20000–40000	0.0	13.8	17.1	11.5	42.4
40000–80000	0.0	2.7	4.2	3.5	10.4

Table 10A. Numbers of "$q\bar{q} \to \gamma + g$" events (divided by 10^3) in Q^2 and x intervals at $L_{\rm int} = 10\,{\rm fb}^{-1}$. The separation efficiencies $\epsilon^{\gamma/{\rm mes}}$ and $\epsilon^{q/g}$ are taken into account

Q^2	x values of a parton				All x
$({\rm GeV}/c)^2$	10^{-4}–10^{-3}	10^{-3}–10^{-2}	10^{-2}–10^{-1}	10^{-1}–10^{0}	10^{-4}–10^{0}
1600–2500	29.1	37.8	51.0	12.0	129.9
2500–5000	9.9	46.2	48.9	7.5	112.4
5000–10000	1.5	10.7	11.9	3.9	27.9
10000–20000	0.1	2.6	2.3	1.7	6.7
20000–40000	0.0	0.7	0.6	0.7	1.9
40000–80000	0.0	0.1	0.2	0.2	0.6

Table 11A. Numbers of "γ–brem" events (divided by 10^3) in Q^2 and x intervals at $L_{\rm int} = 10\,{\rm fb}^{-1}$. The separation efficiencies $\epsilon^{\gamma/{\rm mes}}$ and $\epsilon^{q/g}$ are taken into account

Q^2	x values of a parton				All x
$({\rm GeV}/c)^2$	10^{-4}–10^{-3}	10^{-3}–10^{-2}	10^{-2}–10^{-1}	10^{-1}–10^{0}	10^{-4}–10^{0}
1600–2500	48.5	147.1	177.8	32.5	406.0
2500–5000	17.2	95.0	132.2	27.5	272.0
5000–10000	1.4	12.2	17.0	4.2	34.8
10000–20000	0.0	1.6	2.6	0.9	5.1
20000–40000	0.0	0.3	0.3	0.3	0.9
40000–80000	0.0	0.0	0.1	0.1	0.2

Table 12A. Numbers of "γ–mes" events (divided by 10^3) in Q^2 and x intervals at $L_{\rm int} = 10\,{\rm fb}^{-1}$. The separation efficiencies $\epsilon^{\gamma/{\rm mes}}$ and $\epsilon^{q/g}$ are taken into account

Q^2	x values of a parton				All x
$({\rm GeV}/c)^2$	10^{-4}–10^{-3}	10^{-3}–10^{-2}	10^{-2}–10^{-1}	10^{-1}–10^{0}	10^{-4}–10^{0}
1600–2500	19.9	98.0	102.5	10.2	230.6
2500–5000	4.2	35.6	37.4	4.2	81.4
5000–10000	1.3	4.6	7.4	3.0	16.2
10000–20000	0.0	0.8	0.6	0.5	1.9
20000–40000	0.0	0.1	0.2	0.1	0.3
40000–80000	0.0	0.0	0.01	0.01	0.02

References

1. D. Denegri et al., Summary of the CMS Discovery Potential for the MSSM SUSY Higgses, CMS NOTE 2001/032; S. Abdullin et al., J. Phys. G **28**, 469 (2002), hep-ph/9806366; R. Kinnunen, Higgs physics at LHC, CMS conference report, CMS CR 2002/020
2. P. Aurenche et al., Proceedings of ECFA LHC Workshop, Aachen, Germany, 4–9 October 1990, edited by G. Jarlskog, D. Rein (CERN-Report No 90-10; Geneva, Switzerland 1990), Vol. II
3. UA1 Collaboration, C. Albajar et al., Phys. Lett. B **209**, 385 (1998)
4. UA2 Collaboration, R. Ansari et al., Phys. Lett. B **176**, 239 (1986)
5. CDF Collaboration, F. Abe et al., Phys. Rev. Lett. **68**, 2734 (1992); F. Abe et al., Phys. Rev. D **48**, 2998 (1993); F. Abe et al., Phys. Rev. Lett. **73**, 2662 (1994)
6. D0 Collaboration, F. Abachi et al., Phys. Rev. Lett. **77**, 5011 (1996)
7. D0 Collaboration, B. Abbott et al., Phys. Rev. Lett. **84**, 2786 (2000); D0 Collaboration, V. Abazov et al., Phys. Rev. Lett. **87**, 251805 (2001)
8. P. Aurenche, J. Lindfors, Nucl. Phys. B **168**, 296 (1980)
9. P. Aurenche, A. Douiri, R. Baier, M. Fontannaz, D. Schiff, Phys. Lett. B **140**, 87 (1984)
10. T. Ferbel, W.R. Molzon, Rev. Mod. Phys. **56**, 181 (1984)
11. J.F. Owens, Rev. Mod. Phys. **59**, 465 (1987)
12. E.N. Argyres, A.P. Contogouris, N. Mebarki, S.D.P. Vlassopulos, Phys. Rev. D **35**, 1584 (1987)
13. P. Aurenche et al., Phys. Rev. D **39**, 3275 (1989)
14. E.L. Berger, J. Qiu, Phys. Rev. D **44**, 2002 (1991)
15. J. Huston et al., Phys. Rev. D **51**, 6139 (1995)
16. W. Vogelsang, A. Vogt, Nucl. Phys. B **453**, 334 (1995)
17. W. Vogelsang, M. Whally, J. Phys. G **23**, A1 (1997)
18. J. Huston, ATLAS Note ATL-Phys-99-008, CERN, 1999
19. S. Frixione, W. Vogelsang, CERN-TH/99-247, hep-ph/9908387

20. E706 Collaboration, L. Apanasevich et al., Phys. Rev. Lett. **81**, 2642 (1997)
21. UA6 Collaboration, G. Ballocchi et al., Phys. Lett. B **436**, 222 (1998)
22. A.D. Martin et al., Eur. Phys. J. C **4**, 463 (1998)
23. CTEQ Collaboration, H.L. Lai et al., Eur. Phys. J. C **12**, 375 (2000); see also http://www.phys.psu.edu/ cteq
24. P. Aurenche, M. Fontannaz, S. Frixione, Proceedings of CERN Workshop on Standard Model Physics (and more) at the LHC, section 6.1 (QCD), General features of photon production, Yellow Report CERN-2000-004, 9 May 2000, CERN, Geneva
25. ISR–AFS Collaboration, T. Akesson et al., Zeit. Phys. C **34**, 293 (1987)
26. UA2 Collaboration, J. Alitti et al., Phys. Lett. B **299**, 174 (1993)
27. CDF Collaboration, F. Abe et al., Phys. Rev. D **57**, 1359, 67 (1998)
28. D.V. Bandourin, V.F. Konoplyanikov, N.B. Skachkov, hep-ex/0207028
29. D.V. Bandourin, N.B. Skachkov, Proceedings of XI International Workshop on Deep Inelastic Scattering DIS 2003, St. Petersburg, April 23–27, 2003, edited by V.T. Kim, L.N. Lipatov, p. 546–551, hep-ex/0403024
30. D.V. Bandourin, V.F. Konoplyanikov, N.B. Skachkov, JINR preprint E2-2000-255, hep-ex/0011017
31. M. Dittmar, F. Pauss, D. Zurcher, Phys. Rev. D **56**, 7284 (1997)
32. D.V. Bandourin, V.F. Konoplyanikov, N.B. Skachkov, JINR preprint E2-2000-251, hep-ex/0011012
33. D.V. Bandourin, V.F. Konoplyanikov, N.B. Skachkov, Part. Nucl. Lett. **103**, 34 (2000), hep-ex/0011015
34. M. Dittmar, K. Mazumdar, N. Skachkov, Proceedings of CERN Workshop on Standard Model Physics (and more) at the LHC, section 2.7 (QCD), Measuring parton luminosities and parton distribution functions, Yellow Report CERN-2000-004, 9 May 2000, CERN, Geneva
35. D.V. Bandurin, N.B. Skachkov, Phys. Part. Nucl. **35**, part 1, 66–106 (2004), hep-ex/0304010
36. D.V. Bandurin, N.B. Skachkov, Phys. Atom. Nucl. **67**, N4, 688–692 (2004)
37. D.V. Bandourin, V.F. Konoplyanikov, N.B. Skachkov, JINR Communication E1-2001-261, hep-ex/0108050
38. CMS Electromagnetic Calorimeter Project, Technical Design Report, CERN/LHCC 97–33, CMS TDR 4, CERN, 1997
39. CMS Tracker Project, Technical Design Report, CERN/LHCC 98–6, CMS TDR 5, CERN, 1999
40. D.V. Bandourin, N.B. Skachkov, JINR Communication E2-2001-259, JHEP **04**, 007 (2004), hep-ex/0108051
41. A. Kyriakis, D. Loukas, J. Mousa, D. Barney, CMS Note 1998/088
42. T. Sjostrand, Comp. Phys. Comm. **82**, 74 (1994). Version 6.131 of PYTHIA was used
43. D.V. Bandourin, N.B. Skachkov, JINR Communication E2-2001-260, hep-ex/0109001
44. R. Ball, M. Dittmar, W.J. Stirling, Proceedings of CERN Workshop on Standard Model Physics (and more) at the LHC, section 2 (QCD), Parton distribution functons, Yellow Report CERN-2000-004, CERN, 2000